Combustion and Flame 163 (2016) 281–289

Contents lists available at ScienceDirect

Combustion and Flame

journal homepage: www.elsevier.com/locate/combustflame

Quantifying the enhanced combustion characteristics of electrospray assembled aluminum mesoparticles

Rohit J. Jacob, Boran Wei, Michael R. Zachariah*

Department of Chemical and Bio-molecular Engineering, Department of Chemistry and Biochemistry, University of Maryland, College Park 20742, USA

ARTICLE INFO

Article history:
Received 5 June 2015
Revised 25 September 2015
Accepted 25 September 2015
Available online 29 October 2015

Keywords:
Nano-scale architecture
Nano-aluminum
Burn time
Nitrocellulose
Sintering

ABSTRACT

Aluminum particles have been extensively used to enhance the combustion characteristics of propellant, pyrotechnic and explosive formulations. Unfortunately the relatively high ignition temperatures of aluminum result in severe sintering prior to combustion, leading to early loss of nanostructure and thus a smaller power law exponent for size dependent burning than expected. One such scheme we explore, to defeat sintering, is to create low temperature gas-generation, which helps in breaking up the soft agglomerates before/during combustion. In this article, we characterize the combustion characteristics of electrospray assembled micron scale particles composed of commercial nano-aluminum (ALEX), bound in an energetic polymer matrix composed of nitrocellulose. The nitrocellulose not only acts as a binder for the nanoparticles but also as a dispersant owing to its dissociation at low temperatures (ca. 450 K). Combustion characteristics were measured by direct injection of the electrospray assembled particles into the post flame region of a CH_4/O_2 diffusion flame. We find that the composite meso-particles show an order of magnitude reduction in average burn times when compared to that of the commercial nanoaluminum (ALEX), and are as fast as the shortest nanoparticle burn time. Scanning electron microscopy of quenched post-combustion particles clearly shows smaller sized products in the combustion of electrospray generated composite particles when compared to ALEX powder. This latter point should also lead to a more complete reaction and certainly demonstrates that the concept of using a two-stage reacting system: one at low temperatures to generate gas to separate particles followed by the nominal oxidation reaction is at the least a strategy that is worthy of further exploration.

1. Introduction

Addition of reactive metals to energetic formulations has been extensively studied and practiced over the past five decades [1–3]. Aluminum, owing to its low cost, availability, safety and high energy density, has been one of the focal points of this research. A large body of work has already been undertaken to gauge the benefits of the addition of aluminum particles to energetic formulations and the general consensus is that the addition of aluminum to propellant mixtures improves the combustion stability, energy density and impulse performance [4]. Although the benefits are unambiguous, practical systems have been unable to unlock the maximum potential of aluminum additives. Traditional propellant systems incorporate fine aluminum particles in the range of 10–100 μm, which are protected by an alumina shell (5–20 nm) with a substantially higher melting point (2350 K) compared to the aluminum core (933 K). Such a high melting shell delays the ignition until the temperature rises to the range of 1000–2300 K for particles in the transition regime (10–100 μm) and above 2350 K for larger aluminum particles [5], which correspond to the melting of the shell. Such a delay results in agglomerate formation within the pockets of the oxidizer grains in the propellant and ultimately much larger aluminum droplets, which burn farther from the propellant surface thus reducing the heat feedback and performance. In addition, such large agglomerates increase the slag weight in the combustion products leading to two-phase flow losses.

Much effort has been expended at the mechanistic understanding of the burning of aluminum particles [6]. Large aluminum particles ($>$ 200 μm) are observed to burn in a diffusion-limited regime, following a $D^{1.8}$ dependence. The slightly lower exponent than the expected D^2 is attributed to the presence of oxide caps on the burning particle and violent fragmentation of the same towards the end of the burn. For finer particles, the data is much more scattered and the conclusions consequently more ambiguous. The diameter power dependence for fine particles in the range of 10–14 μm vary from 0.3 to 1 [7], whereas for ultra-fine particles (nanoscale), recent results report a diameter dependency of ~0.3 [8]. Such scatter makes it impossible to model the behavior of a burning aluminum particle across a wide size range [9] and raises questions regarding the mechanistic features that would lead to such low power dependence. Several postulates have been proposed for resolving this conflict. Allen and co-workers

* Corresponding author. Fax: +1 301 314 947.
E-mail address: mrz@umd.edu (M.R. Zachariah).

http://dx.doi.org/10.1016/j.combustflame.2015.09.032
0010-2180/

[10] have suggested that the thermal accommodation coefficient at high temperatures is lower than the assumed value of unity implying that burning nanoparticles might be hotter than expected. This possibility enhances the prospects posited [11] that nanoparticles which are normally in the form of fractal aggregates sinter rapidly, resulting is a larger effective particle size. Recent MD simulations of nanoscale energetics provided a theoretical validation of the rapid sintering concept [12]. The authors argued that upon heating, strong electrical fields generated within the particles lead to enhanced migration of aluminum ions into the protective shell resulting in the transformation of the shell into an aluminum rich, low melting alloy. This transformation led to enhanced coalescence at lower temperatures than the melting point of the protective alumina shell. The authors concluded that for a 100 particle aggregate of 50 nm diameter primaries, the effective coalescence time is $\sim$ 50 ns which is orders of magnitude smaller than the characteristic reaction time ($\sim$10 μs). More recently, experimental validation for this theoretical postulate was presented by Egan et al. [13], where the aggregates of aluminum nanoparticles were rapidly heated within a Dynamic Transmission Electron Microscope (DTEM) which provided high temporal and spatial resolution of the sintering event. Based on their results, sintering of aluminum nanoparticle aggregates were found to be complete on a time scale of $<$ 50 ns. Very recent work by our group on the combustion of size selected nanoparticles of Titanium and Zirconium suggests that once the effects of sintering are accounted for, the diameter dependence of the particle burn time approaches the $\sim D^1$ dependence suggesting that the combustion at the nanoscale is predominantly limited by heterogeneous reactions as expected [14] and that sintering must occur very early in the reaction. What we may conclude is that despite the uncertainty in burning mechanisms, and the diminished power in the scaling law, there appears to be a preponderance of evidence that there is definitely an improvement in going to the nanoscale in terms of burn rate and ignition delay [8,9].

Despite the overall improvement in going to the nanoscale, the fact that the scaling law for burning has a low power dependence suggests that many of the advantages of small scale are not being completely exploited. Combating sintering of metal additives has been a focal point of several recent works owing to the benefits of shorter ignition delays resulting in enhanced heat feedback to the propellant surface, and reduced two-phase flow losses [15,16]. Although the usage of nanoaluminum does increase the burn rate of composite propellants, there are significant difficulties in processing the propellant formulation leading to less than optimal aluminum content, lower friction and impact thresholds and shorter shelf life. Another option, which could circumvent the disadvantages of nanoscale material, would be to develop functionalized micron sized materials, which are modified such that they contribute to the reaction at a much faster time scale than the parent particle. This could be done by modifying the surface of conventional micron sized particles with halides [17], which weakens the shell, or as discussed in this study, bottom up approaches may also be used to package nano-material into micron scale structures [18]. Recent studies in this direction use mechanical activation (Top down) by milling micron sized aluminum particles with gas generators (LDPE), oxidizers (PTFE) [19] or with other metals such as Nickel [20] or Magnesium [21].

Bottom up assembly offers clear advantages with a more direct control of assembly [22,23]. Recent work by our group in employing electrospray assembly/synthesis has found interesting, and in some cases, unexpected benefits in producing energetic fibers [24] and nanothermite composites [18]. In this work, we employ electrospray assembly to generate micron-sized particles (hereon mesoparticles) composed of nano-sized commercial aluminum powder (ALEX) assembled into a mesostructure using nitrocellulose as a binder. The benefits of such an architecture are multifold. In addition to creating a highly accessible, porous structure with a high surface area for reaction (nanoscale characteristic), the generated particles are bound together using an energetic binder, which has a low dissociation temperature. This leads to intra-particle outgassing at the early stages of particle heat up thereby reducing the sintering during combustion. In addition, the generated composite particles are micron sized which should offer processing and handling advantages of the micron scale. Previous works on such mesoscale composites have shown interesting behavior such as lower ignition delay times [25], greater reactivity [18], and high fuel loading capabilities [26]. The basic concept behind this structure is that the addition of low temperature gas-generator (nitrocellulose) should promote primary particle separation and thus decrease sintering. The current work expands these results more quantitavely, gauging the reactivity of such mesoparticles by measuring their burn time in a hot, oxidizing environment. Direct comparisons with that of the parent nanoparticles highlight the de-agglomeration effects of the mesoparticles.

2. Experimental

2.1. Materials

Commercial aluminum nanopowder (ALEX) prepared via exploding wire technique was procured from Argonide Corp. The particles had a core–shelled structure and the primary particle sizes were 50 nm with an active aluminum content of 70%, measured using Thermo Gravimetric Analysis (TGA) [27]. Collodion solution was procured from Sigma Aldrich and contained 4–8 wt% nitrocellulose in an ethanol/diethyl ether mix. The solvent was evaporated off to get the polymer (NC), which was further cut to the required mass.

2.2. Flat flame diffusion burner

In order to evaluate the combustion characteristics we employed a multi element diffusion flat flame burner or Hencken burner [8,13] to provide a high temperature, oxidizing environment for particle combustion with methane as fuel, oxygen as oxidizer and nitrogen as diluent. The flame was kept fuel lean ($\phi \sim 0.3$) so as to keep oxygen as a major constituent in the combustion environment. As shown in Fig. 1a, the particles are injected along the centerline of the burner directly into the products of the flat diffusion flame. The temperature of the oxidizing zone could be varied by changing the reaction stoichiometry and was varied between 900 K and 1500 K as can be seen in Fig. 1b. The major product compositions, predicted by constant enthalpy-pressure calculations in NASA CEA, for each of these flame conditions are outlined in Table 1. Temperature along the burner centerline was mapped using a B-type thermocouple (Omega) consisting of platinum rhodium alloy wires (Pt30Rh and Pt6Rh) with a 0.01 in. junction spot and is plotted in Fig. 1b after correcting for radiation

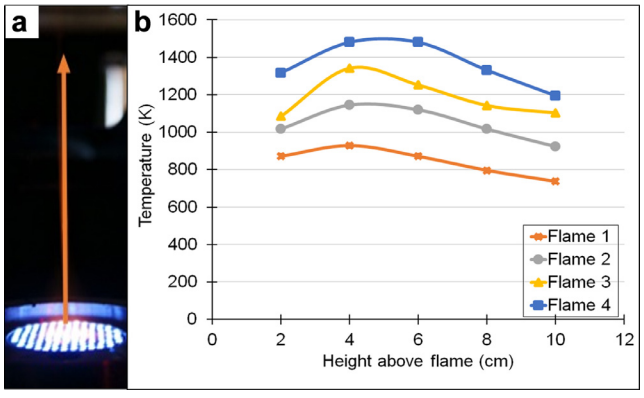

Fig. 1. Multi element diffusion flat flame burner: (a) Burner centerline along which particles are injected into the high temperature, oxidizing zone. (b) Temperature profiles along the burner centerline for different flame stoichiometries.

Table 1
Oxidation zone properties for different flame stoichiometries.

Flame condition	Eq. ratio (T_{ad}, K)	Product fraction: O_2	Product fraction: CO_2	Product fraction: H_2O	Product fraction: N_2
Flame 1	0.21 (1770)	0.49	0.067	0.13	0.30
Flame 2	0.3 (2174)	0.42	0.091	0.18	0.29
Flame 3	0.33 (2212)	0.37	0.094	0.18	0.33
Flame 4	0.41 (2328)	0.29	0.101	0.20	0.38

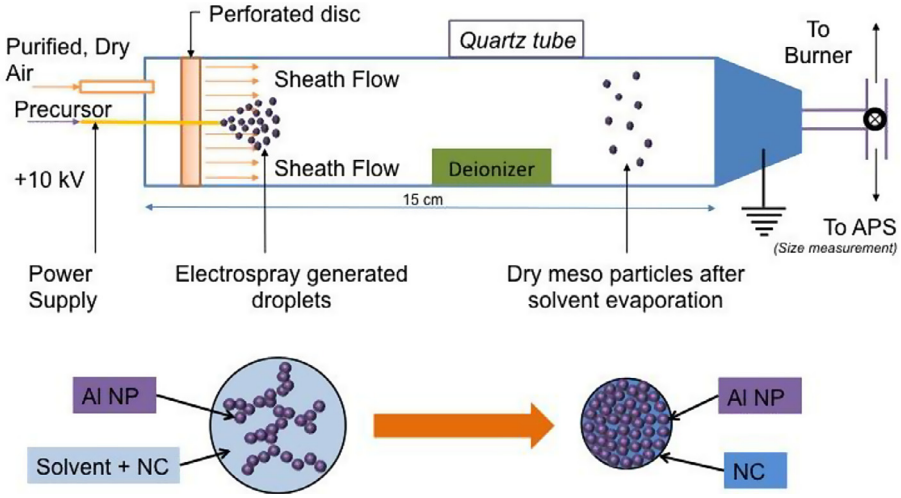

Fig. 2. Electrospray generated mesoparticle aerosolizer.

from the junction spot [28]. Three readings were recorded per position in the oxidizing zone and the average was taken to reduce the error associated with carbon deposition on the fine wire.

2.3. Precursor preparation for mesoparticles

For a typical precursor preparation, 185.6 mg of aluminum nanopowder (containing 70% of active aluminum particles) is weighed and then poured into 1.5 ml of ethanol (99.8%). The mixture is ultra-sonicated for an hour to form a homogenous suspension. After ultra-sonication, 14.4 mg (for 10 wt% NC case) of nitrocellulose was added into the system along with 0.5 ml of ether. The suspension was further magnetically stirred for 24 h to form the final precursor for the electrospray synthesis. Two more precursors compositions were also considered containing 5 and 15 wt% NC respectively so as to gauge the effect of nitrocellulose on the combustion characteristics. Subsequent TEM analysis of the mesoparticles did not show any discernable changes to the oxide shell of the nanoaluminum.

2.4. Electrospray setup and aerosolization

After stirring for 24 h, the precursor was electrosprayed through 23-gauge nozzle (McMaster, I.D. 0.017 in.) connected to a high voltage source at (+) 10 kV to create the electric field required to drive the electrospray process (Fig. 2). The liquid flow rate was controlled with a syringe pump at a feed rate of 4.5 ml/h (7.5 mg/min of mesoparticles). The feed rate and the voltage were empirically selected to provide a stable Taylor cone for droplet generation. In our previous works the mesoparticles were deposited on a substrate where macroscopic harvesting enabled powder sample combustion studies [18]. However for evaluating single mesoparticle combustion and its comparison with nanoaluminum, it was necessary to inject the electrospray stream of mesoparticles directly into the burner. In order to do so, the needle, connected to the high voltage supply, was housed within a chamber with a grounded outlet so as to generate the electric field required to drive the electrospray. The length of the chamber was designed so as to provide sufficient residence time for solvent evaporation in the generated droplets (~15 s in the current setup). Sheath airflow of 1.5 lpm was used as carrier gas to aerosolize the generated droplets and carry them to the combustion zone. A polonium source was incorporated within the chamber, as depicted in Fig. 2, to bring the highly charged droplets to Boltzmann equilibrium charge distribution so as to reduce the losses during transit within the chamber and tubes.

2.5. Nano particle aerosolizer

The mesoparticles are a structural assembly composed of commercial nanoparticles as primaries. So in order to gauge any enhancement, a direct comparison of the combustion characteristics needs to be made between the mesoparticles and the commercial nanoparticles. In order to do so, a powder aerosol generator was built as shown in the Supplemental section (Fig. S1a). The design for the feeder was inspired from the work on coal combustion by Quann et al. [29]. The feeder consisted of a cylindrical powder reservoir (0.18 in. ID × 2 in. length), which was mounted upon a screw feeder connected to a stepper motor. 100 mg of aluminum nanopowder was weighed and vigorously shaken using a vortex mixer to break up large agglomerates before adding into the reservoir. The sheath air (1.5 lpm) entrains the particles from the upper surface of the powder and subsequently enters a 1/8 in. tube which delivers it into the high temperature oxidizing environment. Adjusting the speed of the stepper motor allowed the control of the powder feed rate and was set at 5 mg/min, which offered the steadiest burn at 1.5 lpm.

2.6. Particle size distribution, high-speed videography and electron microscopy

The size distribution of the aerosol before feeding into the burner was measured using an Aerodynamic Particle Sizer Spectrometer (TSI model 3321). The spectrometer uses scattered light from the particles in the aerosol, and has an operation range of 0.5–20 μm. Combustion of the particles was observed using a Phantom high-speed

camera (V12.1) focused directly at the burner centerline. Owing to the extremely small sizes of the particles being studied, we found it necessary to employ a macrolens (Nikon, 105 mm) to get the best resolution while tracking the burning particles. The frame rate used was 10,000–13,000 fps at an exposure of 100–77 μs respectively an aperture of f/2.4. The burn time was calculated by tracking individual particles frame to frame so that the total burn time could be obtained by taking the product of the number of frames and the interval between the frames. The combustion products were quench collected onto metallic stubs and were subsequently analyzed in a Scanning Electron Microscope (Hitachi SU-70 SEM) for final product characterization.

3. Results

3.1. Structure and morphology of commercial aluminum nanoparticles

Commercial aluminum nanopowder is composed of primary particles with a mean diameter of 50 nm. Although the individual particles have a nanoscale dimension, the powder is heavily agglomerated owing to weak Van-der Waals interactions, which leads to characteristically larger agglomerates. A SEM image of the nanopowder is shown in Fig. 3a, which shows an agglomerate composed of fine nanoparticles as primaries. The inset shows a high magnification TEM image of the 50 nm primary particles within the agglomerate. When the powder is aerosolized, the generated aerosol would contain such agglomerates rather than individual primary particles as exemplified by Fig. 3b, which shows the size distribution of the aerosol that is generated using the commercial aluminum powder. The lower detection limit of the instrument was limited to 0.5 μm and hence the complete size distribution down to the nanoscale could not be determined. Even with this limitation, it can be concluded that the commercial powder contains a very wide size distribution with at least two peaks: one at the submicron range and other at approx. 2–3 μm.

3.2. Structure and morphology of electrospray generated mesoparticles

Electrospray generation is a simple one step process in which the liquid precursor is subjected to a electro-hydrodynamic electrical stress, which leads to its breakup into small droplets. Such disintegration is contingent upon the applied electrical stress overcoming the surface tension and viscous stress that try to maintain the integrity of the jet. Depending on the competition between the various stresses, different spraying modes can be produced varying from simple dripping to multiple cone spraying [30]. In this work we employed the cone jet spraying mode owing to the monodisperse nature of the droplets that are generated [31]. The choice of solvent has a significant impact on the structure of the generated particles. The electrospray process generates droplets containing the precursor solution from which the solvent subsequently evaporates leading to the formation of composite mesostructures. As outlined in a recent review by Xie et al. [30], solvents with low vapor pressure have longer evaporation times and therefore lead to particles that have smoother surface morphologies whereas, solvents with high vapor pressure has higher evaporation rates which leads to the formation of particles that exhibit highly porous or textured surface morphologies owing to the lack of rearrangement time for the polymer chains within the droplets. Our objective was to create mesostructures that demonstrated a significantly high surface area, on the same order as that of nanoparticles, but packaged into a micron scale composite. Hence several volatile solvents such as ethanol–ether (3:1), acetone and DMF were tested for the electrospray generation.

The particles generated using ethanol ether mix (3:1) demonstrated a highly spherical structure (Fig. 4a) when compared to the other solvents used (see Supplemental Fig. S2). A closer look at the individual particles for the aforementioned case shows a highly textured surface as shown in the inset of Fig 4a. The key advantage of such a ground up synthesis is that the generated micron sized particles possess approximately the same specific surface area as the primaries comprising the mesoparticles. This implies that the whole mesoparticle structure has the same effective reaction surface area as the nanoparticles, as is also evidenced in the cross-sectional SEM images in Ref. [25]. In Fig. 4b we present the measured size distribution of the electrospray generated nanoparticles, along with a log-normal fit. The resulting size distribution, with a mean size of 1.6 μm, is quite narrow with a standard deviation of 0.37. This is one of the main advantages of using electrospray technique as it generates a near monodisperse aerosol of particles. For comparison we also plot the corresponding self-preserving size distribution (centered at the same peak size) that would be obtained if a normal spray were employed to generate the mesoparticles i.e., without an electric bias [32].

3.3. Combustion characteristics of commercial nanoparticles vs mesoparticles

3.3.1. Visual inspection of the combustion behavior

The representative images of the combustion of both sets of particles are shown in Fig. 5. Fig. 5a shows a long exposure (1/20 s) image of the combustion of nanoaluminum, whereas Fig. 5b represents a similar event recorded at 10,000 fps or 100 μs exposure. As can

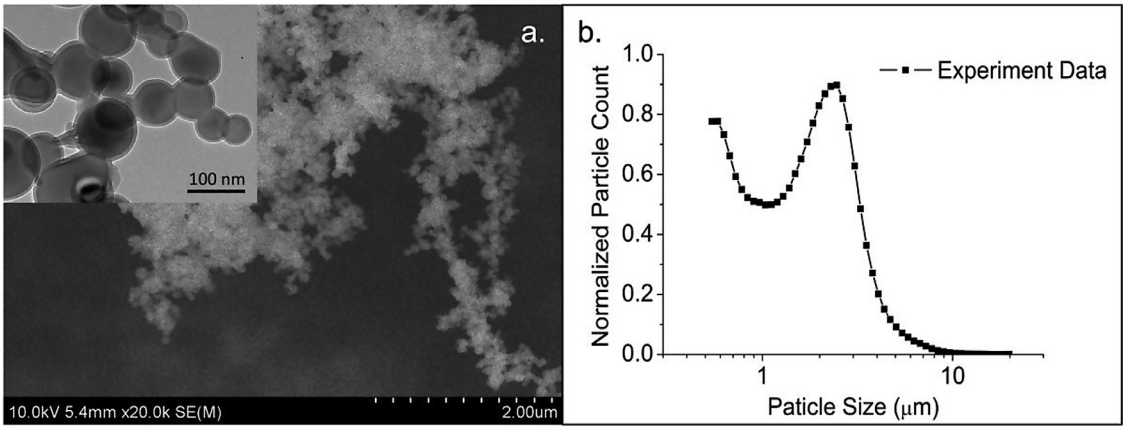

Fig. 3. Morphology and size distribution of commercial aluminum nanopowder: (a) nanopowder agglomerate with high magnification TEM image (inset). (b) Size distribution of the aerosolized nanoaluminum powder.

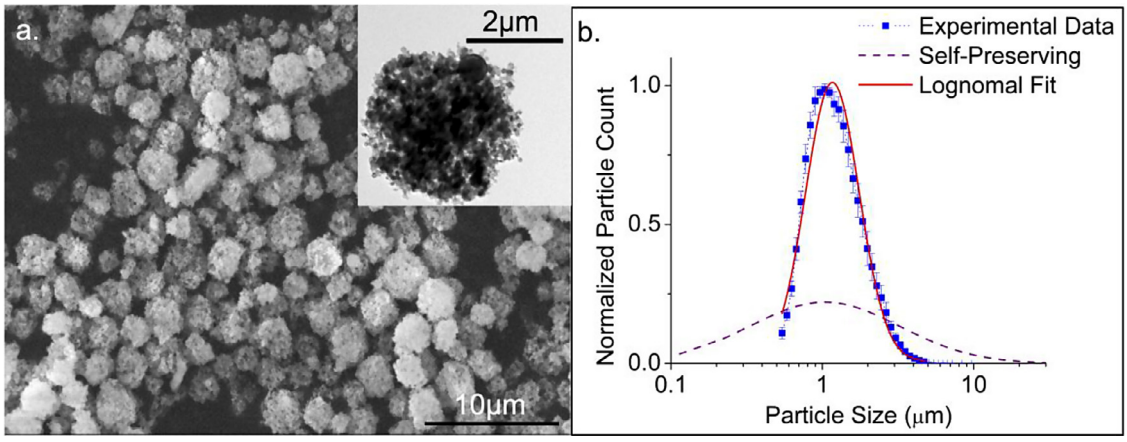

Fig. 4. (a) SEM image of electrospray assembled Al/NC (10 wt%) mesoparticles using ethanol/ether = 3:1 mixture as the solvent, with a high magnification TEM image of a single particle as inset. (b) measured size distribution and comparison with self-preserving distribution.

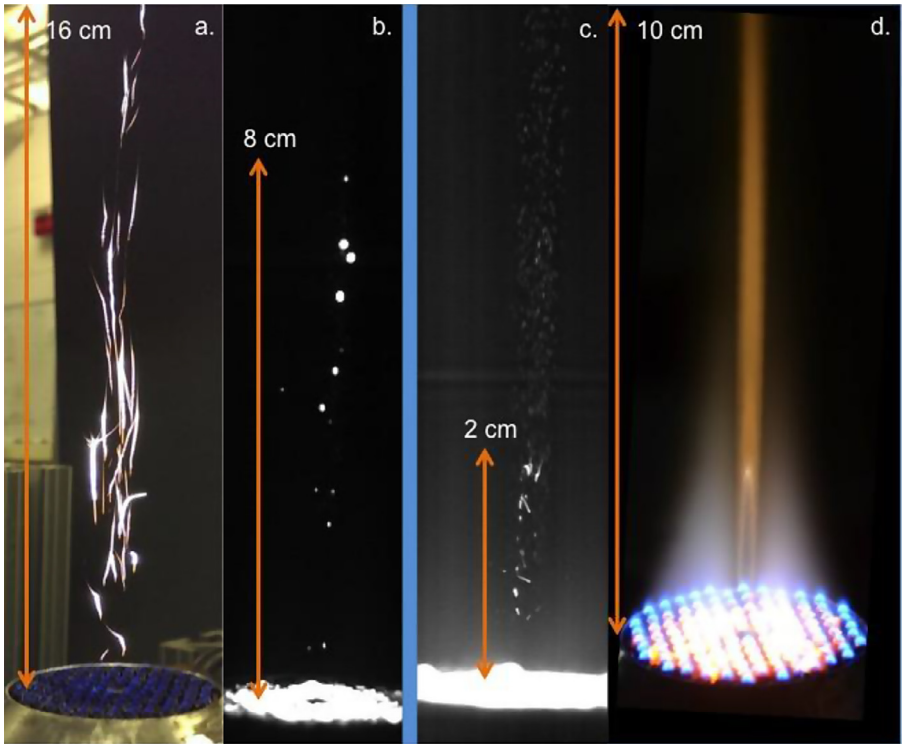

Fig. 5. Combustion images: (a) Nanoaluminum at exposure of 0.05 s. (b) nanoaluminum at exposure of 100 μs. (c) Aluminum mesoparticles at exposure of 83 μs. (d) Aluminum mesoparticle at exposure of 0.5 s; images shown with individual scale bars owing to the differences in magnification during the separate experiments.

be seen from Fig. 5a, combustion of nanoaluminum particles shows a wide range of streak lengths (i.e. burn times). Some very short streaks occurring close to the aerosol outlet at the base of the burner probably represents the population of particles that belong to a much finer size scale, as their ignition temperatures and ignition delays are substantially lower than that of larger particles [8,9]. This latter point also is consistent with sintering, since one expects ignition to be characteristic of the primary particle size and not the size of the aggregate, unless sintering is rapid. In comparison, the electrospray assembled mesoparticles (Fig. 5c, d) show a much smaller burn time as can be seen in Fig. 5c, and are also observed to ignite sooner than the bulk of nanoaluminum particles. Fig. 5d represents an image taken at a longer exposure for the mesoparticles from which the narrow flame shape confirms the narrow range of burn times, certainly much narrower than that found for the nanoaluminum.

3.3.2. Quantifying the burn time of nanoaluminum

From the high-speed images, as shown in Fig 5b, individual particles were tracked throughout its burn and the frame number was used to quantify the burn time. Approximately 100 particles were tracked for each ambient temperature condition corresponding to those outlined in Table 1 and Fig. 1. A histogram plot representing the distribution of burn times for nanoaluminum at Flame 3 condition (from Table 1) is shown in Fig. 6a. As can be seen, the burn time measurements are spread over a wide range of values and have a standard deviation of 6000 μs, with an average of around 4500 μs. From the figure, it is also evident that the majority of burn time measurements are within the 1000 μs bin. Owing to the polydisperse nature of the powder resulting from agglomeration, particle burn times as large as 35,000 μs were observed which skewed the average to a higher value. At this point we note that these measurements of average burn

Please cite this article as: R.J. Jacob et al., Quantifying the enhanced combustion characteristics of electrospray assembled aluminum mesoparticles, Combustion and Flame (2016), http://dx.doi.org/10.1016/j.combustflame.2015.09.032

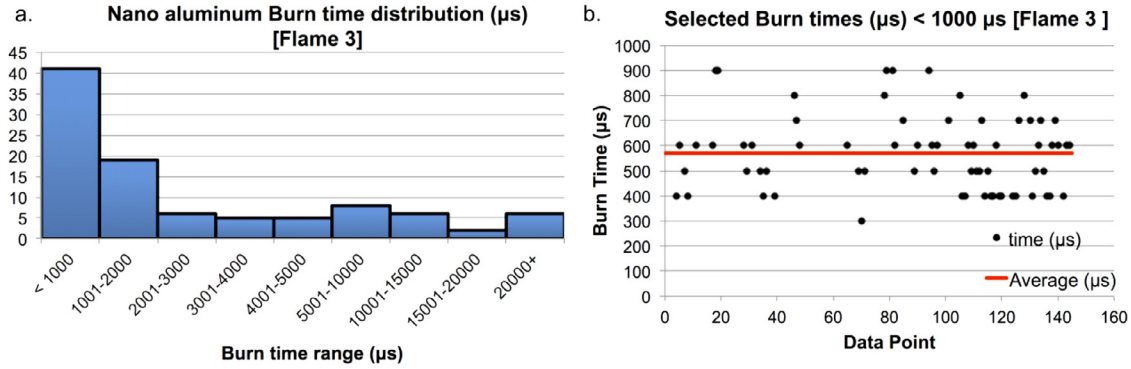

Fig. 6. Burn time plots for nanoaluminum for Flame 3 condition: (a) All data points for nanoaluminum. (b) Selected burn times below 1000 μs for nanoaluminum. Horizontal line representing the average burn time.

Table 2
Average burn time measurements for commercial nanoaluminum powder.

Flame condition →	Flame 1 (841 K)	Flame 2 (1040 K)	Flame 3 (1200 K)	Flame 4 (1360 K)
Nano Al burn time (μs) [*All data points*]	2700 μs	4740 μs	4440 μs	3460 μs
Nano Al burn time (μs) [sub 1000 μs data]	750 μs	663 μs	570 μs	594 μs

time of ALEX nanoparticles (~4500 μs) are consistent with the values published by other researchers on the combustion of nanoaluminum at atmospheric conditions [8,33]. In order to sieve out the outliers, all the values exceeding 1000 μs were discarded from the burn time measurements and the results are plotted in Fig. 6b. With this filtering, the measurements all lie within a narrow range of values with a standard deviation of 150 μs as opposed to 6000 μs when the entire range was considered. The average value of the selected data is found to be ~570 μs, and represents the shortest burn times observed for nanoaluminum combustion. Experimental findings by Bazyn et al. [34] have shown that nanoaluminum burn times are on the order of ~500 μs in a shock tube at 8 atm pressure, 1400 K and 50% O_2 environment. Due to the shock induced break up of the large agglomerates, the shock tube results should reflect the combustion of the smallest aggregates in the aerosol.

Burn time measurements for nanoaluminum are summarized in Table 2 with each flame condition represented by an average temperature obtained from the profile. Also shown are the average burn time estimates based on considering only sub 1000 μs measurements. Although only about 100 burn time measurements were made for each flame condition, we believe the statistical confidence in this measurement, based on the standard deviations, is sufficient to corroborate the arguments regarding the combustion enhancement of the mesoparticles.

3.3.3. Quantifying the burn time of aluminum mesoparticles

A similar procedure as that of the commercial nanoparticles was undertaken for measuring the burn times for the mesoparticles, and the results (all burn time data points) are plotted in Fig. 7. In some cases, owing to the low intensity levels during combustion, we found it necessary to digitally enhance the gain of the video to clearly demarcate the beginning and end of combustion. As can be seen, the burn times of mesoparticles do not display the scatter that the commercial nanoparticles have. The average burn time measured for the Flame 3 condition was measured to be 365 μs, with a standard deviation of 62 μs. We attribute this narrow range of burn times as a direct consequence of the highly monodisperse nature of the mesoparticles.

Burn times and standard deviations measured for mesoparticle combustion in different ambient temperatures are shown in Table 3.

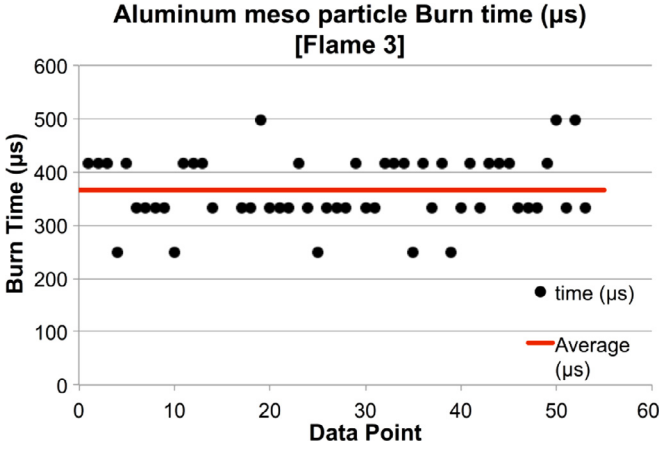

Fig. 7. Burn time scatter plot for aluminum mesoparticles in Flame 3. Horizontal line representing the average burn time.

Similar measurements were also made for mesoparticles made from varying percentages of nitrocellulose (5 and 15 wt% NC) loading in the precursor and are also shown in Table 3. As can be seen, the percentage of nitrocellulose in the composite has little effect on the burn time. In general we see smaller burn times than the nanoparticles (compare with Table 2), the implications of which will be discussed later in the paper.

3.3.4. Product analysis

The idea behind packing commercial nanoparticles into a mesostructure using an energetic gas-generator was to ensure that the low temperature dissociation of the energetic binder (NC) would enhance the dispersion of the nanoparticles thereby reducing sintering at the onset of combustion. In order to confirm if such a phenomenological mechanism is indeed occurring, direct measurements of the particle sizes post combustion were made. For this study the products of combustion were quench collected by rapidly inserting metallic substrates into the post flame region at a height of ~10 cm above the aerosol inlet, and imaged in a Scanning Electron Microscope (SEM). The results are shown in Fig. 8 for both commercial nanoparticles and our mesoparticles. As can be inferred from Fig 8a, commercial nanoparticles do produce some very large spheres, which are a result of a large agglomerates sintering into a much larger droplet, and subsequently burning in the oxidizing environment. Interestingly, for the case of mesoparticles (Fig. 8b), no such large particles were found in the SEM images. Moreover, at a higher magnification, we could observe a much finer population of particles that were common to both commercial nanoparticles and the assembled

Table 3
Average burn time/standard deviation measurements for aluminum mesoparticles.

Flame condition →	Flame 1 (841 K)	Flame 2 (1040 K)	Flame 3 (1200 K)	Flame 4 (1360 K)
Meso Al burn time (μs) [10 wt% NC]	366 μs/72 μs	420 μs/76 μs	365 μs/62 μs	326 μs/83 μs
Meso Al burn time (μs) [5 wt% NC]	302 μs/48 μs	286 μs/49 μs	357 μs/153 μs	324 μs/88 μs
Meso Al burn time (μs) [15 wt% NC]	385 μs/63 μs	405 μs/63 μs	380 μs/51 μs	390 μs/58 μs

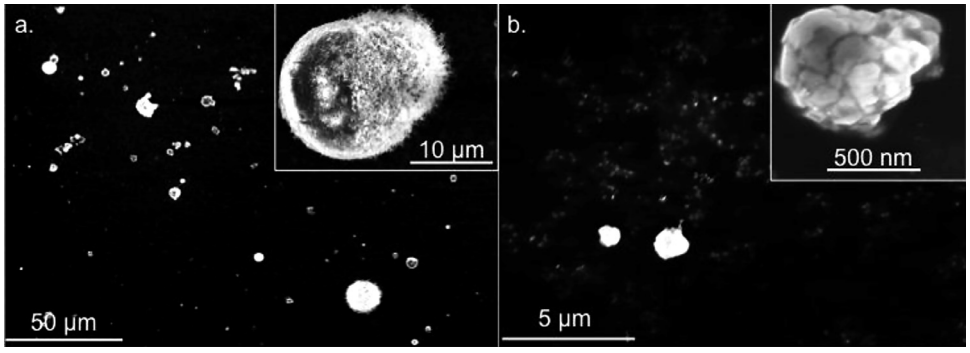

Fig. 8. SEM images of the products collected post combustion: (a) Commercial nanoaluminum with an inset of an individual particle at high magnification. (b) Aluminum mesoparticles with an inset of an individual particle at high magnification.

mesoparticles and is presented in the Supplemental section (Fig. S3). This result implies that our approach to assemble mesoparticles comprised of nanoparticles offers a successful strategy to disintegrate the structure into fine components that burn individually and at a higher burn rate.

4. Discussion

From the size distribution results in Fig. 3, it is clear that the commercial nanopowder (ALEX) has a polydisperse size distribution owing to the weak Van der Waals interactions between the individual nanoparticles leading to the formation of agglomerates [35]. Since ALEX was synthesized using the exploding wire technique, particle collisions during coalescence lead to the formation of the so called hard agglomerates which exhibit intraparticle necking [36] as can be seen in the inset of Fig. 3. Such hard agglomerates are extremely difficult to break therefore any measured property of commercial nanoaluminum particles would inevitably be affected by such agglomerates. Based on the results in [36], such hard agglomerates usually extend to approximately 10 primary particles. Hence the larger agglomerates that we see in the size distributions are aggregates of such hard aggregates. Recent results from high heating rate dynamic TEM experiments [13] show that once an aluminum agglomerate heats up beyond a threshold temperature of approx. 1300 K, coalescence is immediate and occurs on a time scale of tens of nanoseconds which is 3–6 *orders of magnitude* shorter than the measured burn times in this study [13]. This result offers an interesting discussion point to our experiments, since the ambient conditions for Flame 1 and Flame 2 (Fig. 1) are seldom above 1300 K implying that the heat required for coalescence must come from the exothermic oxidation reaction. This means that the reaction would have initiated at some localized hot spots within the agglomerates, and the heat generated from this reaction would subsequently accelerate the coalescence. This results in a characteristically much larger particle, on the order of several micrometers, (Fig. 8a) burning over a much longer duration than what would be expected from a truly nanosized material, as graphically depicted in Fig. 9b [14]. This can be further corroborated by the measurements made for micron sized particles [37] with reported

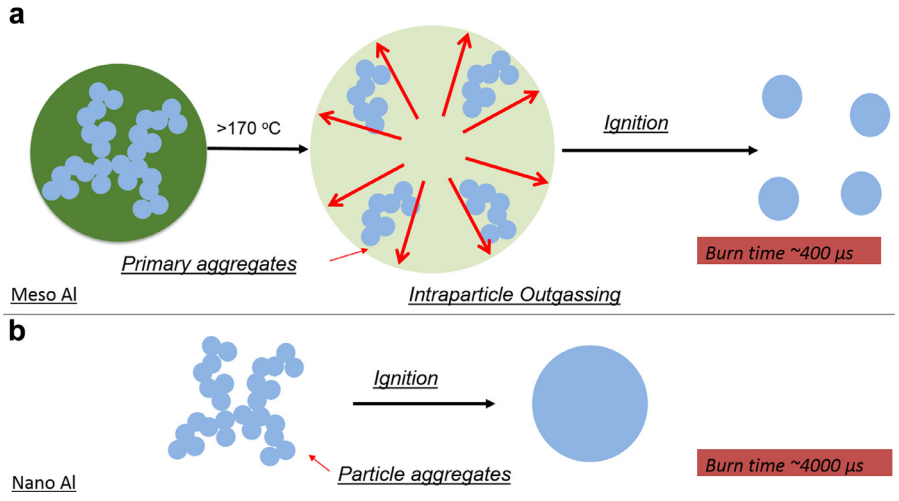

Fig. 9. Pictorial representation of the events leading to combustion of: (a) Aluminum mesoparticles. (b) Commercial aluminum nanoparticles

Please cite this article as: R.J. Jacob et al., Quantifying the enhanced combustion characteristics of electrospray assembled aluminum mesoparticles, Combustion and Flame (2016), http://dx.doi.org/10.1016/j.combustflame.2015.09.032

burn times in the range of 2–5 ms for particles in the range of 2–20 μm.

Electrospray generated mesoparticles on the other hand are packaged into a micron scale composite hence the surface area for heat transfer is greatly reduced although the area available for oxidation remains comparable to the parent nanoparticles owing to the highly intricate mesostructure. Owing to the low decomposition temperature of nitrocellulose (170 °C), the porous structure of the mesoparticles would be exposed early on in the heating. The heat liberated from the oxidation from such exposed regions may contribute directly to cooperative heating of the particle rather than being lost to the surroundings [25]. Such a mechanism would lead to an acceleration of the global reaction owing to the higher temperatures within the composite leading to intraparticle outgassing culminating in the break up of the structural integrity of the composite, shattering into much smaller particles. These smaller fragments could further react without being in close proximity with other fragments till all the fuel is completely oxidized as depicted in Fig. 9a.

From Fig. 5c, we see that some of the streaks in the case of mesoparticles are transverse to the carrier gas flow and this could be a result of the aforementioned outgassing that would lead to sudden impulses which change the trajectory of the particles. The burn time measurements also corroborate such a mechanism, as the measured values for aluminum mesoparticles were in all cases an order of magnitude smaller than what were measured for commercial nanoaluminum. Shock tube measurements of nanoaluminum particles [34] reported a burn time of ~500 μs which are in line with what we observe for the mesoparticles. It must be pointed out that in a shock tube, the particles are ignited behind the reflected shock wave, which implies that the powder is dispersed by a pair of powerful shocks that could successfully break up the large agglomerates. Thus the measurements made would be a function of the smallest aggregates in the powder, which, we believe, would be the aforementioned hard aggregates. The similarity between the shock tube result and the mesoparticles' result in the current study implies that the outgassing is successfully able to disperse the composite structure into smaller fragments albeit in the absence of any shock.

The post-combustion harvesting and imaging of the products of combustion showing the product particles being significantly smaller for mesoparticles than for nanoaluminum is consistent with the conceptual model presented in Fig. 9. Moreover, very recent results [38] incorporating these mesoparticles into composite rocket propellant formulation showed a 35% enhancement in burn rate when compared to the traditional baseline formulation containing 2–3 μm aluminum particles. Such an improvement is attributed to a significant increase in the density and a decrease in size of burning particles on the surface of the propellant. These results imply that the ES assembled mesoparticles can be successfully processed in composite propellant formulations and that the mesostructure is able to successfully disintegrate into smaller fragments that have a lower barrier toward ignition. Such a mechanism subsequently improves the heat feedback to the propellant surface and more importantly the final size of the particles are greatly reduced which would help in the reduction of two phase flow losses in the motor thereby improving the combustion efficiency and specific impulse.

5. Conclusions

To summarize, nanoaluminum has several advantages, over dense micron aluminum, including shorter ignition delay, burn times and lower ignition temperatures, properties that are highly desirable for the enhancement of propellant combustion. However, owing to their extremely high surface area and the highly aggregated state of the unreacted as-purchased particles, pre-reaction sintering results in characteristically much larger particles participating in the actual combustion event. In addition, processing challenges and heat transfer effects encountered for nanoparticles have led to a net detrimental effect on combustion characteristics when compared to micron particles [19]. In this work we attempt to bridge the advantages of nanoscale (high surface area) and micron scale (ease of processing) by packaging the nanoparticles into larger *micron scale* composites using an energetic (Nitrocellulose) as a binder. The energetic binder acts as a low temperature gas generator, which helps to disassemble the soft aggregates into smaller fragments early in the reaction process so that the nanostructure inherent in the initial starting material is more effectively utilized. We find in this work that our assembled mesoparticles burn as fast as the smallest hard aggregates in the nanopowder and has a much narrower distribution of burn times than nanoaluminum. This effectively results in the combustion of the smallest aggregates in the powder precursor leading to an order of magnitude lower burn times and substantially smaller products. This latter point should also lead to a more complete reaction and certainly demonstrates that the concept of using a two-stage reacting system, one at low temperatures to generate gas to separate particles followed by the nominal oxidation reaction, is at the least a strategy that is worthy of further exploration.

Supplementary materials

Supplementary material associated with this article can be found, in the online version, at doi:10.1016/j.combustflame.2015.09.032.

References

[1] E.W. Price, R.K. Sigman, Combustion of Aluminized Solid Propellants, in: V. Yang, T.B. Brill, W.Z. Ren (Eds.), Solid Propellant Chemistry, Combustion and Motor Interior Ballistics, Progress in Astronautics and Aeronautics, vol. 185, AIAA, Virginia, 2000, pp. 663–687. Chapter 2.18.
[2] P.F. Pokhil, A.F. Belyaev, Yu V. Frolov, V.S. Logachev, A.I. Korotkov, Combustion of powdered metals in active media, Report No. FTD-MT-24-551-73 translated from Russian by Foreign Technology Division, Wright Patterson Air Force Base, Ohio, USA, 1973.
[3] R.J. Jacob, G. Jian, P.M. Guerieri, M.R. Zachariah, Energy release pathways in nanothermites follow through the condensed state, Combust. Flame 162 (2015) 258–264.
[4] R.L. Geisler, A global view of the use of aluminum fuel in solid rocket motors, 38th AIAA/ASME/SAE/ASEE Joint Propulsion Conference & Exhibit (2002) paper AIAA 2002-3748.
[5] M.A. Trunov, M. Schoenitz, E.L. Dreizin, Ignition of aluminum powders under different experimental conditions, Propell. Explos. Pyrot. 30 (2005) 36–43.
[6] M.W. Beckstead, Correlating aluminum burning times, Combust. Explo. and Shock Waves 41 (2005) 533–546.
[7] R.J. Gill, C. Badiola, E.L. Dreizin, Combustion times and emission profiles of micron-sized aluminum particles burning in different environments, Combust. Flame 157 (2010) 2015–2023.
[8] T.P. Parr, C. Johnson, D. Hanson-Parr, K. Higa, K. Wilson, Evaluation of advanced fuels for underwater propulsion, 39th JANNAF Combustion Subcommittee Meeting (2003) JSC CD-24 (CD ROM).
[9] Y. Huang, G.A. Risha, V. Yang, R.A. Yetter, Effect of particle size on combustion of aluminum particle dust in air, Combust. Flame 156 (2009) 5–13.
[10] D. Allen, H. Krier, N. Glumac, Heat transfer effects in nano-aluminum combustion at high temperatures, Combust. Flame 161 (2014) 295–302.
[11] K.T. Sullivan, W.A. Chiou, R. Fiore, M.R. Zachariah, In situ microscopy of rapidly heated nano-Al and nano-Al/WO3 thermites, Appl. Phys. Lett. 97 (2010) 133104.
[12] P. Chakraborty, M.R. Zachariah, Do nanoenergetic particles remain nano-sized during combustion? Combust. Flame 161 (2014) 1408–1416.
[13] G.C. Egan, K.T. Sullivan, T. LaGrange, B.W. Reed, M.R. Zachariah, In situ imaging of ultra-fast loss of nanostructure in nanoparticle aggregates, J. Appl. Phys. 115 (2014) 084903.
[14] Y. Zong, R.J. Jacob, S. Li, M.R. Zachariah, Size resolved high temperature oxidation kinetics of nano-sized titanium and zirconium particles, J. Phys. Chem. A 119 (2015) 6171–6178.
[15] V. Babuk, I. Dolotkazin, A. Gamsov, A. Glebov, L.T. De Luca, L. Galfetti, Nanoaluminum as a solid propellant fuel, J. Propul. Power 25 (2009) 482–489.
[16] W.Q. Pang, X.Z. Fan, F.Q. Zhao, W. Zhang, H.X. Xu, H.J. Yu, W.X. Xie, N. Yan, F.L. Liu, Effects of different nano-metric particles on the properties of composite solid propellants, Propell. Explos. Pyrot. 39 (2014) 329–336.
[17] F. Maggi, S. Dossi, C. Paravan, L.T. DeLuca, M. Liljedahl, Activated aluminum powders for space propulsion, Powder Technol. 270 (2015) 46–52.
[18] H. Wang, G. Jian, G.C. Egan, M.R. Zachariah, Assembly and reactive properties of Al/CuO based nanothermite microparticles, Combust. Flame 161 (2014) 2203–2208.
[19] T.R. Sippel, S.F. Son, L.J. Groven, S.S. Zhang, E.L. Dreizin, Exploring mechanisms for agglomerate reduction in composite solid propellants with polyethylene inclusion modified aluminum, Combust. Flame 162 (2015) 846–854.

Please cite this article as: R.J. Jacob et al., Quantifying the enhanced combustion characteristics of electrospray assembled aluminum mesoparticles, Combustion and Flame (2016), http://dx.doi.org/10.1016/j.combustflame.2015.09.032

[20] J.L. Cheng, H.H. Hng, H.Y. Ng, P.C. Soon, Y.W. Lee, Synthesis of sub-micron nickel particles coated onto aluminum powders via a modified polyol process, Met. Mat. Intern. 14 (2008) 583–587.
[21] Y. Aly, V.K. Hoffman, M. Schoenitz, E.L. Dreizin, Reactive, Mechanically alloyed Al center dot Mg powders with customized particle sizes and compositions, J. Propul. Power 30 (2014) 96–104.
[22] S.H. Kim, M.R. Zachariah, Enhancing the rate of energy release from nanoenergetic materials by electrostatically enhanced assembly, Adv. Mater. 16 (2004) 1821–1825.
[23] N.A. Clayton, K.S. Kappagantula, M.L. Pantoya, S.C. Kettwich, S.T. Iacono, Fabrication, characterization, and energetic properties of metallized fibers, ACS Appl. Mater. Interfaces 6 (2014) 6049–6053.
[24] S. Yan, G.Q. Jian, M.R. Zachariah, Electrospun nanofiber-based thermite textiles and their reactive properties, ACS Appl. Mater. Interfaces 4 (2012) 6432–6435.
[25] H.Y. Wang, G.Q. Jian, S. Yan, J.B. DeLisio, C. Huang, M.R. Zachariah, Electrospray formation of gelled nano-aluminum microspheres with superior reactivity, ACS Appl. Mater. Interfaces 5 (2013) 6797–6801.
[26] X.Y. Li, P. Guerieri, W.B. Zhou, C. Huang, M.R. Zachariah, Direct deposit laminate nanocomposites with enhanced propellant properties, ACS Appl. Mater. Interfaces 7 (2015) 9103–9109.
[27] S. Chowdhury, K. Sullivan, N. Piekiel, L. Zhou, M.R. Zachariah, Diffusive vs explosive reaction at the nanoscale, J. Phys. Chem. C 114 (2010) 9191–9195.
[28] R.M. Fristrom, A.A. Westenberg, Flame Structure, McGraw Hill, New York, U.S.A., 1965.
[29] R.J. Quann, M. Neville, M. Janghorbani, C.A. Mims, A.F. Sarofim, Mineral matter and trace-element vaporization in a laboratory-pulverized coal combustion system, Environ. Sci. Technol. 16 (1982) 776–781.
[30] J.W. Xie, J. Jiang, P. Davoodi, M.P. Srinivasan, C.H. Wang, Electrohydrodynamic atomization: A two-decade effort to produce and process micro-/nanoparticulate materials, Chem. Eng. Sci. 125 (2015) 32–57.
[31] M. Cloupeau, B. Prunetfoch, Electrostatic spraying of liquids in cone-jet mode, J. Electrostat. 22 (1989) 135–159.
[32] S.K. Friedlander, Smoke Dust and Haze, Fundamentals of aerosol dynamics, Oxford University Press, New York, U.S.A., 2000.
[33] C.D. Kong, Q. Yao, D. Yu, S.Q. Li, Combustion characteristics of well-dispersed aluminum nanoparticle streams in post flame environment, Proc. Combust. Inst. 35 (2015) 2479–2486.
[34] T. Bazyn, H. Krier, N. Glumac, Combustion of nanoaluminum at elevated pressure and temperature behind reflected shock waves, Combust. Flame 145 (2006) 703–713.
[35] D.H. Tsai, R.A. Zangmeister, L.F. Pease, M.J. Tarlov, M.R. Zachariah, Gas-phase ion-mobility characterization of SAM-functionalized Au nanoparticles, Langmuir 24 (2008) 8483–8490.
[36] C.D. Yarrington, S.F. Son, T.J. Foley, S.J. Obrey, A.N. Pacheco, Nano aluminum energetics: The effect of synthesis method on morphology and combustion performance, Propell. Explos. Pyrot. 36 (2011) 551–557.
[37] C. Badiola, E.L. Dreizin, Combustion of micron-sized particles of titanium and zirconium, Proc. Combust. Inst. 34 (2013) 2237–2243.
[38] G. Young, H.Y. Wang, M.R. Zachariah, Application of nano-aluminum/nitrocellulose mesoparticles in composite solid rocket propellants, Propell. Explos. Pyrot. 40 (2015) 413–418.

Please cite this article as: R.J. Jacob et al., Quantifying the enhanced combustion characteristics of electrospray assembled aluminum mesoparticles, Combustion and Flame (2016), http://dx.doi.org/10.1016/j.combustflame.2015.09.032